J Mater Sci: Mater Electron (2015) 26:8267–8271
DOI 10.1007/s10854-015-3490-5

Fabrication of $SrAl_2O_4:Eu^{2+}$ films on Si substrates via metal–organic solution

Yuguo Yang[1] · Bing Liu[1] · Yuanyuan Zhang[1] · Xianshun Lv[1] · Lei Wei[1] · Xuping Wang[1]

Received: 31 May 2015 / Accepted: 11 July 2015 / Published online: 15 July 2015

Abstract $SrAl_2O_4:Eu^{2+}$ films were fabricated on the Si substrates by metal–organic solution deposition method and subsequent treatment up to 1100 °C. The phase and microstructure of the obtained films were characterized by DTA-TG, XRD, SEM and AFM. The composition of the film was confirmed by XPS. The luminescence properties of the films were measured by spectrophotometer. The effect of annealing temperature on the structure and luminescence was studied. It showed that the films had the pure monoclinic phase and the depth about 2 μm. Under the excitation of 254 nm, $SrAl_2O_4:Eu^{2+}$ films exhibited an intense green emission band peaking at 528 nm, which originates from the $4f$–$5d$ transition of the Eu^{2+} ions. The quenching temperature of the emission is about 400 K. The results indicated that the $SrAl_2O_4:Eu^{2+}$ films have good potential for use as a green phosphor for displays and/or white light emitting diodes.

1 Introduction

Strontium aluminates activated by Eu^{2+} with long afterglow, such as $Sr_4Al_{14}O_{25}$ [1], $SrAl_2O_4$ [2], $Sr_3Al_2O_6$ [3], and $Sr_4Al_2O_7$ [4], have been studied extensively in recent years because of their excellent properties including high quantum efficiency [5], long persistence of phosphorescence and good stability [6]. In the strontium aluminates hosts, Eu^{2+} ions usually show broad band luminescence originating from the $4f^65d^1 \rightarrow 4f^7$ transitions. The interaction of the $4f$ orbitals with their surrounding ions is weak, while the $5d$ orbitals are exposed to the surroundings and therefore the $4f^7 \rightarrow 4f^65d^1$ transitions are strongly influenced by the chemical environment of Eu^{2+}. It is known that the covalency increases with decreasing Al content in the series of Sr-aluminates [7]. As a result, the emission of Eu^{2+} in strontium aluminates hosts can vary from ultraviolet to red, depending on the Al/Sr ratio. And $SrAl_2O_4:Eu^{2+}$ phosphors often show green emission when they are excited by the ultraviolet light [2, 8–10].

The films play an important role in some technological applications, such as microelectronic devices [11], magnetic storage media [12], and surface coating [13]. For example, a luminescence layer on the dye-sensitized solar cell (DSSC) composing of down-conversion phosphor materials has the ability to transform higher energy photons into visible photons, which extends light absorption and enhances photovoltaic performance of DSSC [14]. In addition, the phosphor films have advantages of higher lateral resolution from smaller grains, better thermal stability, reduced out gassing and better adhesion to solid substrates [15]. Therefore, for various industrial applications, it is important to study the properties of phosphors in the form of film.

Synthesis from a solution affords excellent chemical stoichiometry and compositional homogeneity, thus reduces the required diffusion path length [16]. Moreover, films deposited by metal–organic solution deposition method (MOSD) are of great and increasing interest for a wide number of materials ranging from metals to insulators because of advantages of large area deposition with good thickness uniformity, precise control of the stoichiometry, and simple equipment [17]. In the present work, we report on the fabrication and optical properties of $SrAl_2O_4:Eu^{2+}$ films on Si substrates by MOSD. Film structure and

✉ Xuping Wang
wangxp@sdas.org

[1] New Materials Research Institute, Shandong Academy of Sciences, Jinan 250014, People's Republic of China

morphological characterization have been carried out using X-ray diffraction (XRD), scanning electron microscopy (SEM), and atomic force microscopy (AFM).

2 Experiments

The $SrAl_2O_4:Eu^{2+}$ metal–organic solution was prepared using strontium chloride ($SrCl_2{\cdot}6H_2O$), aluminum isopropoxide ($C_9H_{21}AlO_3$), and europium chloride ($EuCl_3{\cdot}6H_2O$) as starting materials. The doping concentration of Eu^{2+} is 2 mol%. At first, stoichiometric amounts of strontium chloride and aluminum isopropoxide were dissolved in ethyl alcohol. The mixed solution was stirred and refluxed at room temperature, and then the desired amount of europium chloride was added for doping and hydrolysis. The resulting mixtures were further stirred for 30 min to yield clear and homogeneous solution, which served as the coating solution after aging at room temperature. The obtained sols were transparent and were dropped onto silicon wafer substrate and spun at 2000 rpm. After being deposited by spin coating, the films were dried at 300 °C in an oven. These coating and drying procedures were repeated 15 times to obtain a desirable film thickness, and the resulting films were annealed in the reducing atmosphere of active carbon at temperatures of 900, 1000 and 1100 °C for 2 h.

The different thermal analysis (DTA) and thermo gravimetric (TG) analysis were measured by the NETZSCH STA 449C thermal analyzer. The XRD patterns of thin films were examined using a Japan RigaKu D/max-g X-ray diffractometer system with graphite monochromatized Cu Kα irradiation. The surface morphology of thin films was observed by AFM (Innova, Veeco) and SEM (S-4800, Hitachi) attached with energy dispersive X-ray spectroscopy (XPS). The luminescence was performed on a HitachiF-7000 spectrophotometer equipped with a 150 W xenon lamp as the excitation source. The decay curves were obtained from a Lecroy Wave Runner 6100 digital oscilloscope (1 GHz) using a tunable laser (pulse width = 4 ns, gate = 50 ns) as excitation source (Continuum Suncite OPO). A FJ427-A1 thermally stimulated spectrometer was used to reveal the afterglow behavior.

3 Results and discussion

Figure 1 gives the DTA-TG curves of $SrAl_2O_4:Eu^{2+}$ phosphor films. There are three regions of mass loss in the TG curve, corresponding to the three exothermic peaks in the DTA curve. The first region originates from the dehydration of the precursor. The second region is due to the pyrolysis of organics. The third region relates to the formation and crystallization of $SrAl_2O_4:Eu^{2+}$. Figure 2 shows the XRD patterns of $SrAl_2O_4:Eu^{2+}$ phosphor films

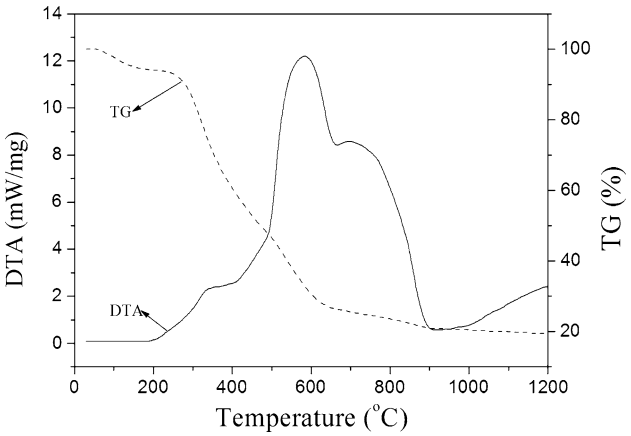

Fig. 1 DTA-TG curves of $SrAl_2O_4:Eu^{2+}$ precursor

annealed at 900, 1000 and 1100 °C for 2 h. All of reflection planes are well according with the JCPDS card No. 74-0794, which indicates the formation of monoclinic phase $SrAl_2O_4$. With the increases of annealing temperature, the diffraction peaks become stronger and sharper, reflecting greater crystallization. No other significant changes are observed. No impurity phase can be observed in the XRD patterns. This fact clearly implies that the little amount of doped Eu^{2+} ions have no effects on the $SrAl_2O_4$ phase composition. $SrAl_2O_4$ adopt a stuffed tridymite-type structure consisting of a corner sharing AlO_4 tetrahedral which connect together to form six-member rings. Each oxygen ion is shared by two aluminum ions so that each tetrahedron has one net negative charge. The charge balance is achieved by the large divalent Sr^{2+}, which occupies interstitial site within the tetrahedral framework [18].

Figure 3 presents the surface morphology of $SrAl_2O_4:Eu^{2+}$ films annealed at 1100 °C for 2 h. As shown in

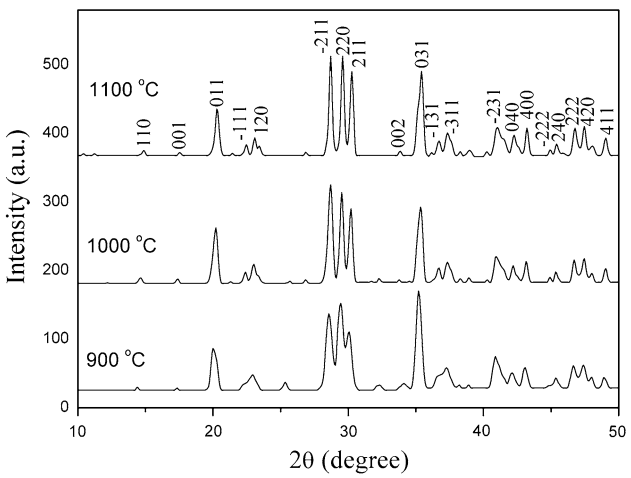

Fig. 2 XRD patterns of $SrAl_2O_4:Eu^{2+}$ films annealed at different temperatures

Fig. 3a, b, the surface of obtained $SrAl_2O_4:Eu^{2+}$ film is smooth and has some micro–pinholes. This is further confirmed by the AFM measurements (Fig. 3d). The AFM results show that the $SrAl_2O_4:Eu^{2+}$ films exhibit homogeneous microstructures consisting of small and large grains with a statistical roughness, root mean square of 28 nm approximately. Figure 3c shows the cross-sectional view, suggesting that the compact $SrAl_2O_4:Eu^{2+}$ films have the depth about 2 μm.

Further evidence of the composition is obtained by the XPS. Figure 4 shows the XPS spectra of $SrAl_2O_4:Eu^{2+}$ films annealed at 1100 °C for 2 h. As shown in Fig. 4a, peaks corresponding to O 2*s* and O 1*s*, Al 2*p* and Al 2*s*, Sr 3*d* and Sr $3p_{3/2}$ can be observed. Figure 4b gives the peaks corresponding to Eu^{2+} $3d_{5/2}$ and Eu^{2+} $3d_{3/2}$, indicating that Eu^{3+} has been reduced to be Eu^{2+} successfully. There is no the XPS peaks corresponding to the Eu^{3+}, which demonstrates to the complete reduction of Eu^{3+}.

In the $SrAl_2O_4$ host, there are two nonequivalent strontium sites with the same coordination number and similar average Sr–O distance, and the difference of these two sites is only the slight distortion of their square planes [19]. As a result, the Eu^{2+} centers are expected to show similar luminescence properties because of the similar local environments of Eu^{2+} ions substituting different Sr^{2+} ions. Figure 5 shows the excitation and emission spectra of $SrAl_2O_4:Eu^{2+}$ films. Figure 5a shows the excitation spectrum of $SrAl_2O_4:Eu^{2+}$ film annealed at 1100 °C for 2 h by monitoring 528 nm emission. As seen from the excitation spectrum, a relatively wide absorption in the range of 200–450 nm appears. Furthermore, four distinguished absorption peaks at 254, 308, 349 and 410 nm emerge in the broad excitation bands, which correspond to the crystal field splitting of the Eu^{2+} *d*-orbital. In $SrAl_2O_4$, the 5*d* levels of the Eu^{2+} ions are located below the ^6P_J state of the $4f^{7*}$ configuration due to the strong crystal field strength, thus creating a broadband luminescence owing to the allowed $4f^6 5d \rightarrow 4f^7$ transition [20]. Upon the excitation of 254 nm, spectra of $SrAl_2O_4:Eu^{2+}$ films annealed at 900, 1000 and 1100 °C for 2 h consist of the single green emitting band with the maximum at 528 nm, which originates from the electric-dipole allowed 4*f*–5*d* transition of the Eu^{2+} ions [21]. All spectra have the same peak position but different emission intensity, by comparison, between the films obtained from various annealed temperatures, indicating the same Eu^{2+} surroundings and different crystallinity. This is according with the XRD results. As shown in Fig. 2, with the increases of annealed temperature, the

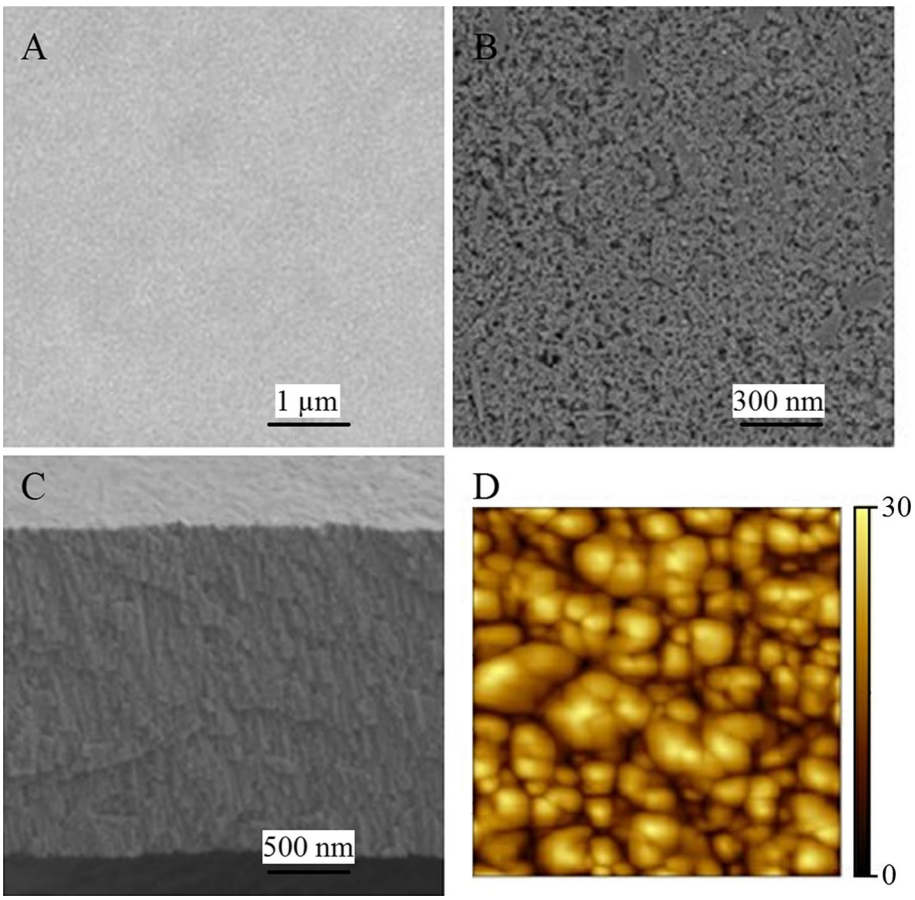

Fig. 3 SEM images (**a** and **b**), cross-sectional view (**c**), and AFM image (**d**) of $SrAl_2O_4:Eu^{2+}$ films annealed at 1100 °C

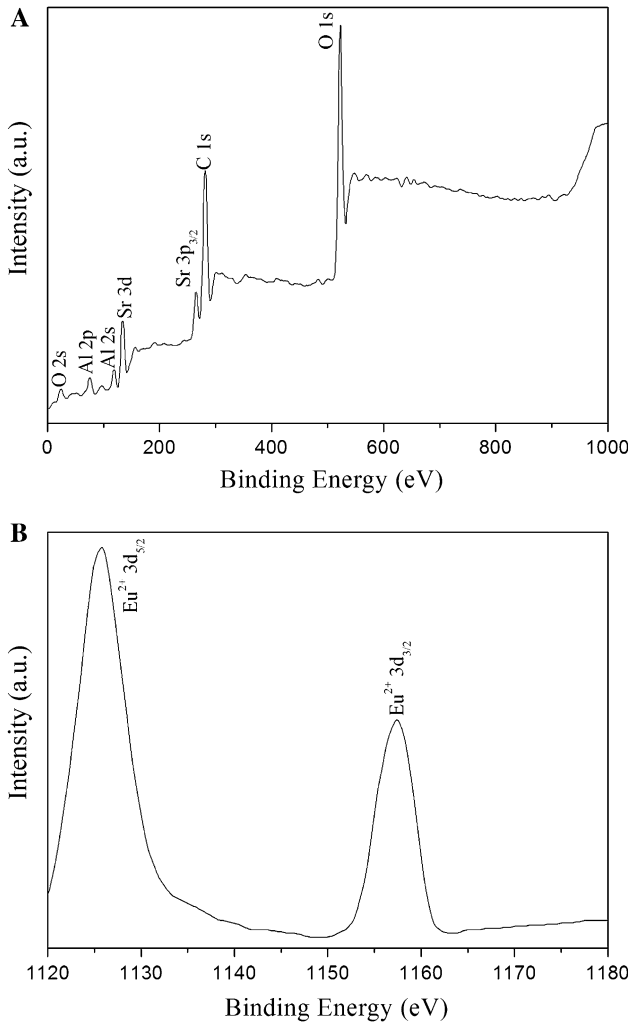

Fig. 4 XPS spectra of $SrAl_2O_4$:Eu^{2+} films annealed at 1100 °C

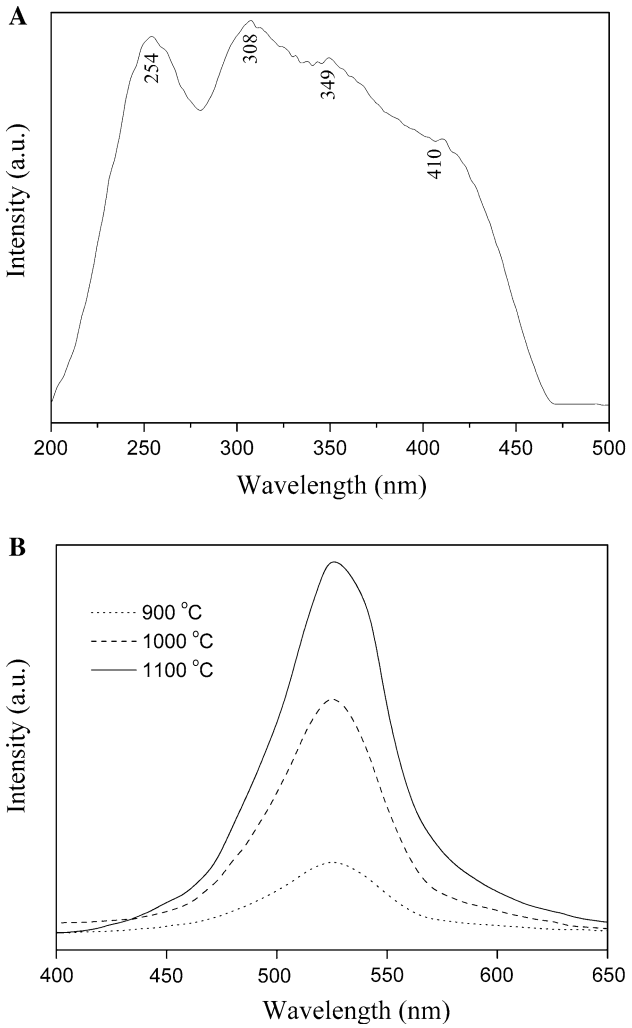

Fig. 5 Excitation (**a**, 1100 °C) and emission (**b**) spectra of $SrAl_2O_4$:Eu^{2+} films annealed at different temperatures

crystallinity increases, but the films maintain the pure monoclinic $SrAl_2O_4$ phase, which induces the increases of emission intensity and the same peak positions. In addition, it should be noted that there is no emission bands coming from the Eu^{3+}, suggesting the Eu^{3+} ions have been reduced to be Eu^{2+} ions completely. This is according with the XRS measurements.

In Fig. 6, the temperature dependence of the intensities of the $4f^65d$ emission for $SrAl_2O_4$:Eu^{2+} films annealed at 1100 °C is plotted. As the $4f^65d$ level is thermally populated, the fast parity allowed emission from this state takes over as is typically observed for Eu^{2+} in host lattices where the $4f^65d$ is situated just above the $^6P_{7/2}$ state. In the temperature range of 285–360 K, the emission intensity is nearly constant. Above 360 K, temperature quenching sets in and the quenching temperature of the emission is about 400 K. The quenching temperature is defined as the temperature at which the emission intensity is reduced to be 50 % of the initial intensity. The decreases of the emission

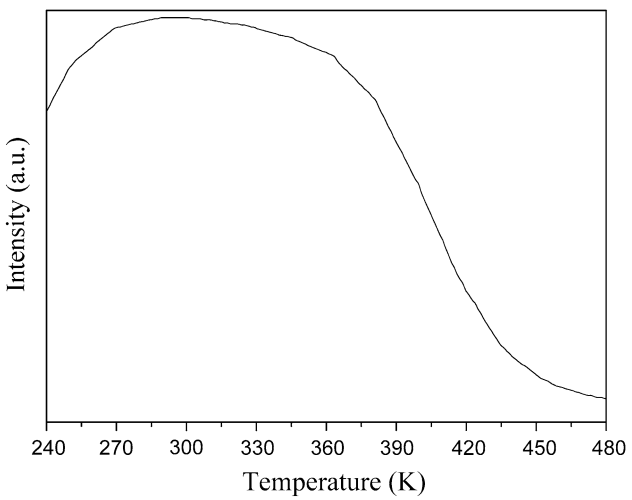

Fig. 6 Dependence of emission intensity on temperature of $SrAl_2O_4$:Eu^{2+} films annealed at 1100 °C

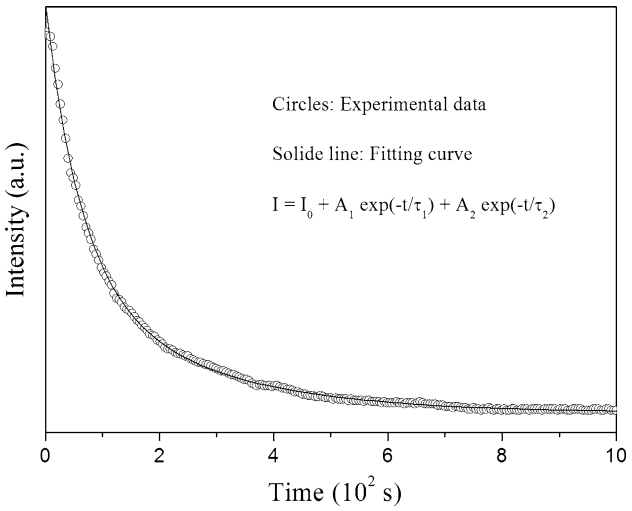

Fig. 7 Decay curve of $SrAl_2O_4:Eu^{2+}$ films annealed at 1100 °C

intensity are due to the electron–phonon interaction between both the ground state and excited states of the luminescence center at high temperature [22].

Figure 7 shows the decay curve of $SrAl_2O_4:Eu^{2+}$ films annealed at 1100 °C. It can be seen that the films show the long persistence. The decay curve indicates that the decay process involves two regimes of an initial rapid-decaying process and a subsequent slow-decaying process. The initial rapid decay corresponds to the intrinsic lifetime of Eu^{2+}, and the long decay of the afterglow due to thermal trapping–detrapping of charge carriers [23]. The decay curve well fits the bio-exponential decay function as follows: $I = I_0 + A_1 \exp(-t/\tau_1) + A_2 \exp(-t/\tau_2)$, where I is the photoluminescence intensity, I_0, A_1, A_2 are the constants, t is the time, τ_1 and τ_2 are the decay constants for exponential components [24]. The decay lifetimes (τ) can be calculated as $\tau = (A_1\tau_1^2 + A_2\tau_2^2)/(A_1\tau_1 + A_2\tau_2)$ [25]. The calculated lifetime is about 236 s.

4 Conclusions

In summary, we synthesized $SrAl_2O_4:Eu^{2+}$ films successfully on the Si substrates by metal–organic solution deposition and subsequent treatment up to 1100 °C. It showed that the films had the pure monoclinic phase and the depth about 2 μm. Under the excitation of 254 nm, $SrAl_2O_4:Eu^{2+}$ films exhibited an intense green emission band peaking at 528 nm originating from the 4*f*–5*d* transition of the Eu^{2+} ions. The quenching temperature of the *d*–*f* emission is about 400 K. The results indicated that the $SrAl_2O_4:Eu^{2+}$ films have good potential for use as a green phosphor for displays and/or white light emitting diodes.

Acknowledgments This work is supported financially by the National Science Foundation of China (Grant Nos. 51102158, 51202135 and 51302158), the Science and Technology Develop Project in Shandong Province (Grant No. 2013GGX10203), Natural Science Foundation of Shandong Province (Grant No. ZR2014EMQ004), and Youth Foundation of Shandong Academy of Sciences (Grant Nos. 2013QN011, 2014QN027 and 2014QN028).

References

1. N. Thompson, P. Murugaraj, C. Rix, D.E. Mainwaring, J. Alloys. Compd. **537**, 147 (2012)
2. H.R. Zhang, Z.P. Xue, B.F. Lei, H.W. Dong, H.M. Zhang, S.Q. Deng, M.T. Zheng, Y.L. Liu, Y. Xiao, Opt. Mater. **36**, 1802 (2014)
3. Y.M. Tian, P. Zhang, Z.T. Zheng, Y.S. Chai, Mater. Lett. **73**, 157 (2012)
4. S.J. Kim, H. Won, N. Hayk, C.W. Won, D.Y. Jeon, A.G. Kirakosyan, Mater. Sci. Eng. B **176**, 1521 (2011)
5. B. Smets, J. Rutten, G. Hoeks, J. Verlijsdonk, J. Electrochem. Soc. **136**, 2119 (1989)
6. F.C. Palilla, A.K. Levine, M.R. Tomkus, J. Electrochem. Soc. **115**, 642 (1968)
7. S.Y. Kaya, E. Karacaoglu, B. Karasu, Ceram. Int. **38**, 3701 (2012)
8. C. Zollfrank, S. Gruber, M. Batentschuk, A. Osvet, F. Goetz-Neunhoeffer, S. Dittrich, J. Grabow, H.-D. Kurland, F.A. Muller, Acta Mater. **61**, 7133 (2013)
9. E. Shafia, M. Bodaghi, S. Esposito, A. Aghaei, Ceram. Int. **40**, 4697 (2014)
10. D.S. Kshatri, A. Khare, J. Alloys. Compd. **588**, 488 (2014)
11. Q. Man, W. Sun, F. Yang, C. Qiu, Y. Zhao, G. Hu, J. Mater. Sci. Mater. Electron. **25**, 1269 (2014)
12. W. Wang, Q.X. Zhu, M.M. Yang, R.K. Zheng, X.M. Li, J. Mater. Sci. Mater. Electron. **25**, 1908 (2014)
13. K. Muthukrishnan, M. Vanaraja, S. Boomadevi, R.K. Karn, J.B.B. Rayappan, V. Singh, K. Pandiyan, J. Mater. Sci. Mater. Electron. **26**, 1908 (2015)
14. W.Z. He, T.S. Atabaev, H.K. Kim, Y.-H. Hwang, J. Phys. Chem. C **117**, 17894 (2013)
15. D.P. Norton, Mater. Sci. Eng. R **43**, 139 (2004)
16. B. Liu, X.P. Wang, Y.Y. Zhang, X.S. Lv, Y.G. Yang, Ionics **20**, 1795 (2014)
17. Y.G. Yang, X.P. Wang, B. Liu, Surf. Interface Anal. **46**, 109 (2014)
18. M. Ayvacıkli, Z. Kotan, E. Ekdai, Y. Karabulut, A. Canimoglu, J.G. Guinea, A. Khatab, M. Henini, N. Can, J. Lumin. **144**, 128 (2013)
19. F. Clabau, X. Rocquefelte, S. Jobic, P. Deniard, M.-H. Whangbo, A. Garcia, T. Le Mercier, Chem. Mater. **17**, 3904 (2005)
20. Y. Liu, C.-N. Xu, J. Phys. Chem. B **107**, 3991 (2003)
21. X.Q. Xing, D.Y. Ling, L. Tan, J. Mater. Sci. Mater. Electron. **25**, 4774 (2014)
22. B.F. Lei, K. Machida, T. Horikawa, H. Hanzawa, Chem. Lett. **40**, 140 (2011)
23. P. Huang, Q.C. Zhang, C. Cui, J. Li, Opt. Mater. **33**, 1252 (2011)
24. F.J. Wei, Q.L. Jia, J. Mater. Sci. Mater. Electron. **26**, 262 (2015)
25. Y.X. Liu, A.Y. Lan, Y. Jin, G.Q. Chen, X. Zhang, Opt. Mater. **40**, 122 (2015)